Received: 16 November 2017 | Revised: 12 December 2017 | Accepted: 13 December 2017

DOI: 10.1002/aoc.4264

FULL PAPER

WILEY Applied Organometallic Chemistry

Polymer complexes. LXX. Synthesis, spectroscopic studies, thermal properties and antimicrobial activity of metal(II) polymer complexes

Sh. M. Morgan[1] | A. Z. El-Sonbati[2] | M. A. El-Mogazy[2]

[1] Environmental Monitoring Laboratory, Ministry of Health, Port Said, Egypt

[2] Chemistry Department, Faculty of Science, Damietta University, Damietta, Egypt

Correspondence
A. Z. El-Sonbati, Chemistry Department, Faculty of Science, Damietta University, Damietta, Egypt.
Email: elsonbatisch@yahoo.com

The monomer 3-allyl-5-(phenylazo)-2-thioxothiazolidine-4-one (HL) was prepared by the reaction of allyl rhodanine with aniline through diazo-coupling reaction. Reaction of HL with Ni(II) or Co(II) salts gave polymer complexes (**1–8**) with general stoichiometries $[M(HL)(Cl)_2(OH_2)_2]_n$, $[M(HL)(O_2SO_2)(OH_2)_2]_n$, $[M(L)(O_2NO)(H_2O)_2]_n$ and $[M(L)(O_2CCH_3)(H_2O)_2]_n$ (where M = Ni(II) or Co(II)). The structures of the polymer complexes were identified using elemental analysis, infrared and electronic spectra, molar conductance, magnetic susceptibility, X-ray diffraction and thermogravimetric analysis. The interaction between the polymer complexes and calf thymus DNA showed a hypochromism effect. HL and its polymer complexes were tested against bacterial and fungal species. Co(II) polymer complex **2** is the most effective against *Klebsiella pneumoniae* and is more active than penicillin. The results showed that Ni(II) polymer complex **5** is a good antibacterial agent against *Staphylococcus aureus* and *Pseudomonas aeruginosa*. Molecular docking was used to predict the binding between the monomer with the receptors of prostate cancer (PDB code: 2Q7L Hormone) and breast cancer (PDB code: 1JNX Gene regulation). Coats–Redfern and Horowitz–Metzger methods were applied for calculating the thermodynamic parameters of HL and its polymer complexes. The thermal activation energy of decomposition for HL is higher than that for the polymer complexes.

KEYWORDS
antimicrobial activity, calf thymus DNA, polymer complexes, thermal analysis, thermodynamic parameters

1 | INTRODUCTION

Interest in coordination chemistry is increasing continuously with the preparation of organic ligands containing an allyl group and such interest is much multiplied when the ligands have biological importance.[1,2] The biochemistry and coordination chemistry of allyl heterocyclic compounds have attracted increased interest due to their chelating ability and their pharmacological applications.

Transition metal polymer complexes are of particular interest due to their various applications.[3–6] Heterocyclic azo dyes attract considerable interest and play an important role in the development of chemistry. A literature survey shows subtle work to synthesize and characterize azo dyes, and also their metal complexes which are widely used in various fields such as biological studies.[7–12]

Over the past few years, the study of rhodanine compounds has been an active area because of their

importance in applied academic researches and their diverse applications such as metal extracting agents,[13] analytical reagents,[14] pharmacological compounds,[15] solar cells[16] and biosensors.[17] Derivatives after substituting various groups in rhodanine also have excellent chemiluminescence and fluorescence performance.[18,19]

The chemistry of nickel has received considerable attention due to the discovery that nickel is an essential metal in antibacterial and antifungal activities.[20] Nickel complexes play an important role in biological systems and there are a number of nickel enzymes.[20,21] In addition, nickel complexes are attracting nowadays increasing interest in the research field of bioinorganic chemistry and there are many reports regarding Ni(II) complexes with antimicrobial, antibacterial, antifungal and antiproliferative properties.[22–24] Also, Co(II) complexes have attracted attention for the thermal stability, coordination chemistry and biological activity of some complexes for which structural information was obtained using spectrochemical and magnetochemical techniques; due to Co(II) showing d^7 arrangement, it can have four-coordinate tetrahedral and six-coordinate octahedral stereochemistry.[25–28]

Allyl rhodanine azo compounds are a subject of growing interest and may have numerous applications, and azo rhodanine compounds containing oxygen, sulfur and nitrogen donor atoms are of great interest because of their great versatility as ligands.[1,2] Because of the presence of several potential donor atoms, they have ability and flexibility to coordinate in either deprotonated or neutral form.

The present paper describes the chelation behavior of 3-allyl-5-(phenylazo)-2-thioxothiazolidine-4-one (HL) monomer towards some ions of Ni(II) and Co(II). Molecular docking was used to predict the binding between the monomer with the receptors of prostate cancer (PDB code: 2Q7L Hormone) and breast cancer (PDB code: 1JNX Gene regulation). The structures of the studied Ni(II) and Co(II) polymer complexes were elucidated using elemental analyses, infrared (IR) and UV–visible spectra, magnetic moment, molar conductance, X-ray diffraction and thermal analysis. The antimicrobial activities of HL and its Ni(II) and Co(II) polymer complexes are discussed. Calf thymus DNA binding of HL and its polymer complexes was studied using absorption spectra. In addition, the thermodynamic parameters were calculated using the Coats–Redfern and Horowitz–Metzger methods.

2 | EXPERIMENTAL

2.1 | Materials and Reagents

3-Allyl-2-thioxothiazolidin-4-one and aniline were bought from Aldrich. 2,2′-Azobisisobutyronitrile (AIBN) was purified by dissolving in hot ethanol and filtering. $NiSO_4{\cdot}6H_2O$, $CoSO_4{\cdot}7H_2O$, $MCl_2{\cdot}6H_2O$ (M = Ni(II) and Co(II)), $M(NO_3)_2{\cdot}6H_2O$ (M = Ni(II) and Co(II)) and $M(CH_3COO)_2{\cdot}\,_4H_2O$ (M = Ni(II) and Co(II)) were obtained from Sigma Aldrich. Organic solvents (diethyl ether, dimethylformamide (DMF), dimethylsulfoxide (DMSO) and ethanol) were bought from BDH. Calf thymus DNA (CT-DNA) was acquired from SRL (India).

2.2 | Preparation of HL Monomer

Monomer (HL) was synthesized by the well-established standard method (Scheme 1).[4,20,29] The resulting solid HL was recrystallized from ethanol and then dried in a vacuum desiccator over anhydrous calcium chloride. Analysis: found for HL monomer ($C_{12}H_{11}N_3OS_2$) (%): C, 52.11; H, 4.09; N, 15.31; S, 23.51; calculated (%): C, 51.99; H, 3.97; N, 15.16; S, 23.11.

2.3 | Preparation of Poly[3-allyl-5-(phenylazo)-2-thioxothiazolidine-4-one] (PHL) Homopolymer

PHL homopolymer was prepared by free radical initiation of HL monomer (0.5 mol) using 0.1% (w/v) AIBN as initiator and DMF (50 ml) as solvent for 6 h. The polymer product was precipitated by pouring in distilled water and dried in a vacuum oven for several days at 40 °C. The PHL homopolymer was characterized using ^1H NMR analysis.

2.4 | Preparation of Polymer Complexes

Polymer complexes were prepared by refluxing Ni(II) and Co(II) salts (0.001 mol) with HL (0.001 mol) in 20 ml of

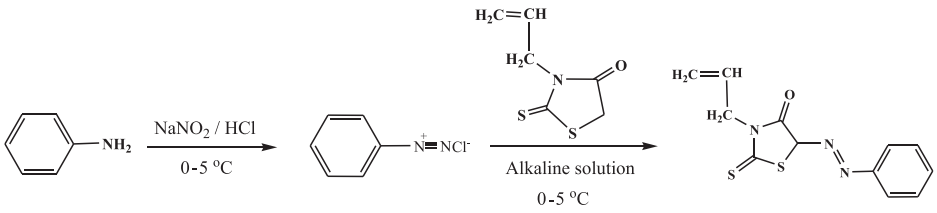

SCHEME 1 Synthesis of monomer (HL)

DMF as a solvent and 0.1% (w/v) AIBN as initiator, and the resulting mixture was heated at reflux for *ca* 8 h. The hot solution was precipitated by pouring in large excess of distilled water containing dilute hydrochloric acid, to remove the metal salts that were incorporated into the polymer complexes. The polymer complexes (**1**–**8**; Table 1) were filtered, washed with water and dried in a vacuum oven at 40 °C for several days.

2.5 | DNA Binding

The binding of the monomer and polymer complexes to CT-DNA was studied using absorption spectra.[20] Electronic absorption spectra were obtained using a 1 cm quartz cuvette at room temperature by fixing the concentration of compound (1×10^{-3} M), while progressively increasing the concentration of CT-DNA. The intrinsic binding constant (K_b) of the monomer and polymer complexes with CT-DNA was determined.[20,28]

2.6 | Biological Activity

For this investigation, the agar well diffusion method was applied.[12,28] The antibacterial activity was tested on nutrient agar medium against three local Gram-positive bacterial species (*Enterococcus faecalis*, *Bacillus cereus* and *Staphylococcus aureus*) and three local Gram-negative bacterial species (*Pseudomonas aeruginosa*, *Klebsiella pneumoniae* and *Escherichia coli*). Also, the antifungal activity of the monomer and polymer complexes was tested against three local fungal species on DOX agar medium (yeast *Candida albicans*, *Aspergillus niger* and *Fusarium oxysporum*). The concentrations of each solution of monomer and polymer complexes were 150, 100 and 50 μg ml in DMF. Utilizing a sterile cork borer (10 mm in diameter), wells were made in agar plates previously seeded with the test microorganism. An amount of 200 μl of each compound was applied in every well. The agar plates were kept at 4 °C for at least 30 min to allow the diffusion of the compound into the agar medium. The plates were then incubated at 37 °C for bacteria and 30 °C for fungi. The diameters of inhibition zones were measured after 24 h and 7 days for bacteria and fungi, respectively, taking into consideration the control values (DMF). Miconazole was used as antifungal standard drug and penicillin as antibacterial standard drug.[20,28]

2.7 | Analytical Measurements

Elemental microanalyses of the compounds for C, H, S and N were conducted with an automatic analyser (CHNS Vario ELIII, Germany). The ^{1}H NMR spectra were obtained with a JEOL FX90 Fourier transform spectrometer with DMSO-d_6 as the solvent and using tetramethylsilane (TMS) as an internal standard. Mass spectra were recorded using the EI technique at 70 eV with a Hewlett-Packard MS-5988 GS-MS. IR spectra were recorded as KBr discs using a PerkinElmer 1340 spectrophotometer. UV–visible spectra of the compounds were recorded in nujol mulls using a Unicom SP 8800 spectrophotometer. The molar conductance was measured with a Sargent Welch Scientific Co. (Skokie, IL, USA) instrument. The magnetic moments of the prepared solid complexes wre determined at room temperature using the Gouy method. Mercury(II) (tetrathiocyanato)cobalt(II), [Hg{Co(SCN)$_4$}], was used for the calibration of the Gouy tubes. Magnetic moments were calculated using the equation $\mu_{eff} = 2.84\ [Tc_M{}^{coor}]^{1/2}$. Thermogravimetric analysis (TGA) was conducted with a Simultaneous Thermal Analyzer (STA) 6000 system, in the temperature range from 30 to 800 °C at a heating rate of 10 °C min^{-1} under dynamic nitrogen atmosphere. X-ray diffraction (XRD) analysis of compounds was conducted with an X-ray diffractometer in the range 2θ = 4–80°.[30] This analysis was carried out using Cu K_α radiation. The applied voltage and the tube current were 40 kV and 30 mA, respectively. The diffraction peaks in powder spectra were

TABLE 1 Elemental analyses and magnetic moment of Ni(II) and Co(II) polymer complexes **1**–**8**

Complex	μ_{eff} (B.M.)	Found (calcd) (%) C	H	N	S	M
$[Ni(HL)(Cl)_2(H_2O)_2]_n$ $C_{12}H_{15}N_3O_3S_2Cl_2Ni$ (**1**)	3.25	32.35 (32.53)	3.25 (3.39)	9.18 (9.49)	14.31 (14.46)	13.77 (13.26)
$[Co(HL)(Cl)_2(H_2O)_2]_n$ $C_{12}H_{15}N_3O_3S_2Cl_2Co$ (**2**)	4.46	32.39 (32.51)	3.27 (3.39)	9.24 (9.48)	14.19 (14.45)	13.22 (13.31)
$[Ni(HL)(O_2SO_2)(H_2O)_2]_n$ $C_{12}H_{15}N_3O_7S_3Ni$ (**3**)	3.46	30.66 (30.79)	3.08 (3.21)	8.68 (8.98)	20.25 (20.53)	12.79 (12.55)
$[Co(HL)(O_2SO_2)(H_2O)_2]_n$ $C_{12}H_{15}N_3O_7S_3Co$ (**4**)	4.92	30.64 (30.77)	3.15 (3.21)	8.74 (8.98)	20.39 (20.52)	12.64 (12.59)
$[Ni(L)(O_2NO)(H_2O)_2]_n$ $C_{12}H_{14}N_4O_6S_2Ni$ (**5**)	3.22	33.22 (33.28)	3.13 (3.24)	12.69 (12.94)	14.58 (14.79)	13.77 (13.56)
$[Co(L)(O_2NO)(H_2O)_2]_n$ $C_{12}H_{14}N_4O_6S_2Co$ (**6**)	4.72	33.17 (33.26)	3.14 (3.23)	12.77 (12.94)	14.55 (14.78)	13.77 (13.61)
$[Ni(L)(O_2CCH_3)(H_2O)_2]_n$ $C_{14}H_{17}N_3O_5S_2Ni$ (**7**)	3.29	39.04 (39.10)	3.86 (3.96)	9.54 (9.77)	14.57 (14.89)	14.04 (13.66)
$[Co(L)(O_2CCH_3)(H_2O)_2]_n$ $C_{14}H_{17}N_3O_5S_2Co$ (**8**)	4.40	39.04 (39.08)	3.84 (3.95)	9.45 (9.77)	14.64 (14.89)	13.83 (13.71)

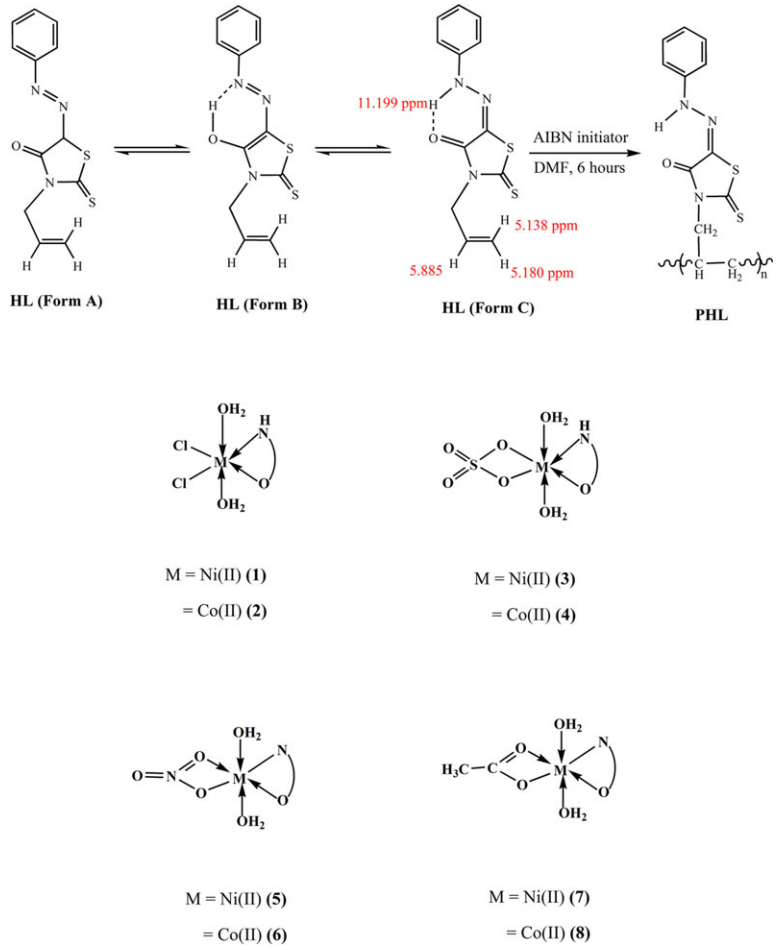

FIGURE 1 Structures of monomer and its polymer complexes

indexed and the lattice parameters were determined with the aid of the CRYSFIRE computer program.[31] The value of interplanar spacing, *d*, and Miller indices, *hkl*, for each diffraction peak were determined using the CHEKCELL program.[32]

Docking calculations were carried out on receptors of the androgen receptor prostate cancer mutant H874Y ligand binding domain bound with testosterone and a TIF2 box3 coactivator peptide 740-753 (PDB code: 2Q7L Hormone) and crystal structure of the BRCT repeat region from the breast cancer associated protein BRCA1 (PDB code: 1JNX Gene regulation).[3,28] Data were statistically analysed for variance using SPSS software version 17 and the least significant difference at 0.05 level using one-way analysis of variance.

3 | RESULTS AND DISCUSSION

3.1 | Structures of Monomer and Polymer Complexes

HL was synthesized by the diazotization of aniline with allyl rhodanine. The elemental analysis data obtained were in good agreement with the stoichiometry of the HL monomer. The monomer can exist in two tautomeric forms, azo enol form (Figure 1, form B) and keto hydrazone form (Figure 1, form C).

HL exhibits bands at *ca* 26 425 cm^{-1} (CS) (n → π*), *ca* 30 640 cm^{-1} (CO) (n → π*) and 40 400 cm^{-1} (phenyl ring) (π–π*). It has been reported that the azo derivatives exhibited a strong band in the range 37 000–35 550 cm^{-1} whereas hydrazone showed a strong band at *ca* 31 250 cm^{-1}.[20]. However, HL gave a characteristic band at *ca* 30 650 cm^{-1} for the hydrazone form (Figure 1, form C).

Elemental analysis data for the polymer complexes are summarized in Table 1. It is found that two types of polymer complexes are formed. For the first type, the monomer behaves as a neutral and contains two/one anions (chloride/sulfate ion) (polymer complexes with equivalent anions (**1**–**4**)):

$NiCl_2{\cdot}6H_2O$	+ HL	→	$[Ni(HL)(Cl)_2(H_2O)_2]_n$
$CoCl_2{\cdot}6H_2O$	+ HL	→	$[Co(HL)(Cl)_2(H_2O)_2]_n$
$NiSO_4{\cdot}6H_2O$	+ HL	→	$[Ni(HL)(O_2SO_2)(H_2O)_2]_n$
$CoSO_4{\cdot}7H_2O$	+ HL	→	$[Co(HL)(O_2SO_2)(H_2O)_2]_n$

For the second type, the monomer behaves as a monobasic anion (nitrate or acetate ion) (polymer complexes with half equivalent anions (**5**–**8**)):

$Ni(NO_3)_2{\cdot}6H_2O$ →	+	HL $[Ni(L)(O_2NO)(H_2O)_2]_n + HNO_3$
$Co(NO_3)_2{\cdot}6H_2O$ →	+	HL $[Co(L)(O_2NO)(H_2O)_2]_n + HNO_3$
$Ni(CH_3COO)_2{\cdot}4H_2O$ →	+	HL $[Ni(L)(O_2CCH_3)(H_2O)_2]_n + CH_3COOH$
$Co(CH_3COO)_2{\cdot}4H_2O$ →	+	HL $[Co(L)(O_2CCH_3)(H_2O)_2]_n + CH_3COOH$

The general formulae for the polymer complexes is $[M(HL)(Cl_2$ or $O_2SO_2)(OH_2)_2]_n$ and $[M(L)(O_2NO$ or $O_2CCH_3)(OH_2)_2]_n$ (where M = Ni(II) or Co(II)). The high decomposition temperature of all polymer complexes as well as their insolubility in common organic solvents, but soluble in DMF and DMSO, suggest the polymeric nature of all polymer complexes.

The elemental analysis results show 1:1 (metal:monomer) stoichiometry for all the polymer complexes and the results are in good agreement with the general formulae (Table 1). The molar conductivities (Λ_m) of 10^{-3} M solutions of the Ni(II) and Co(II) polymer complexes in DMSO at 25 °C were measured, and were found to be non-electrolytic in nature with values in the range 3.4–7.8 Ω^{-1} cm^2 mol^{-1}. The formation of HL and its polymer complexes and bonding modes were inferred from characteristic band positions in IR spectra.

Elemental analysis of HL, as detailed in Section 2.2, indicates that the monomer has the molecular formula $C_{12}H_{11}N_3OS_2$. The mass spectrum of the monomer exhibits a peak at 277 amu conforming to the formula ($C_{12}H_{11}N_3OS_2$) as shown in Figure S1. It is obvious that the molecular ion peaks are in good agreement with the suggested empirical formulae as determined from elemental analyses (Table 1). The ion at m/z = 277 fragmented to a stable peak at m/z = 261 by loss of oxygen atom as shown in Scheme 2 (structure I). The peaks corresponding to various fragments of HL monomer appeared at m/z = 176 (structure II), 149 (structure III), 91 (structure IV) and 77 (structure V) by loss C_4H_5S, CHN, CSN and N atoms, respectively.

The ^{1}H NMR spectrum of HL supports the occurrence of the form depicted in Figure 1. The ^{1}H NMR spectrum of the monomer was recorded in DMSO-d_6 using TMS as the internal standard. The broad signal at *ca* 11.199 ppm was assigned to intramolecular hydrogen bonded proton of NH (hydrazone) (Figure S2a) which disappeared in the presence of D_2O (Figure S2b). These results are in agreement with those obtained by Diab *et al.*[2] where proton of NH (hydrazone) showed a signal at *ca* 11.4 ppm. The protons of the aromatic ring resonate downfield in the range 7.045–7.393 ppm.

The ^{1}H NMR spectrum of HL showed the expected peaks and pattern of the vinyl group (CH_2=CH), i.e. 5.885 ppm for the vinyl CH proton and 5.138 ppm (*cis*) and 5.180 ppm (*trans*) for the vinyl CH_2 protons; these peaks disappeared on polymerization. This indicates that

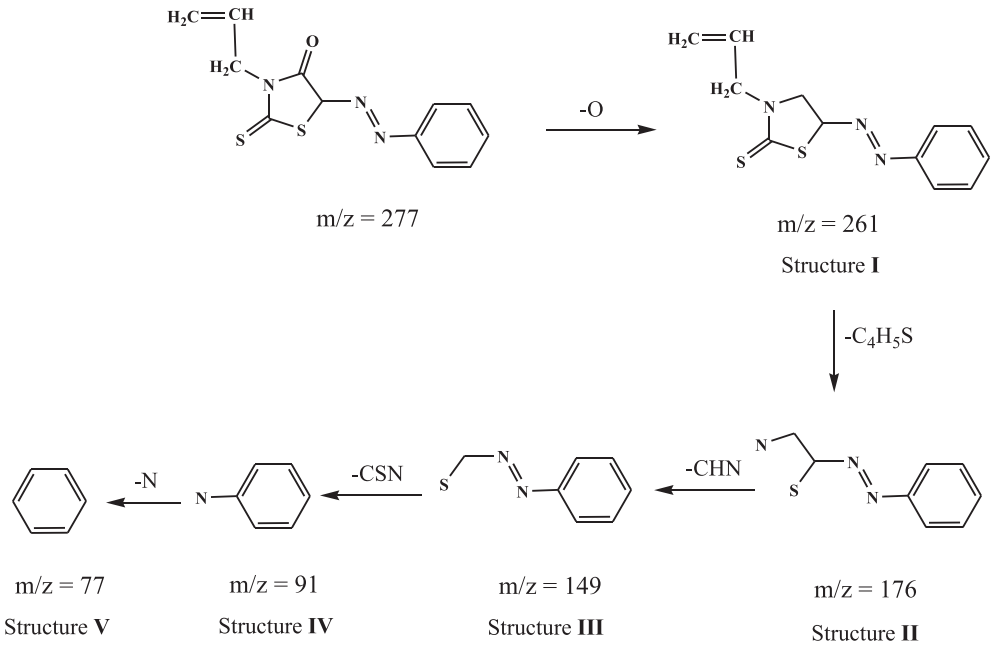

SCHEME 2 Fragmentation patterns of monomer

the polymerization of HL occurs at the vinyl group.[2] It is worth noting that the rest of the proton spectra of HL and PHL remain almost without change.

Molecular docking aims to achieve an optimized conformation for both protein and drug with relative orientation between them such that the free energy of the overall system is minimized.[33,34] In this context, we used molecular docking between HL (forms A–C) and the receptors of prostate cancer and breast cancer. The data showed a favourable arrangement between HL (forms A–C) and the receptors of prostate cancer and breast cancer. The interaction curves are shown in Figures 2–4 and the calculated energy and some parameters associated with the selected anticancer receptors are listed in Table 2. In general a more negative charge represents a more stable interaction, where the estimated free energy of binding, the estimated inhibition constant (K_i) and the interaction surface area reveal the most favoured binding.[28] So, the obtained data show a more favourable interaction between HL (forms A–C) and the receptor of 2Q7L (prostate cancer) than the receptor of 1JNX (breast cancer) (Table 2). The HB plot curves explain the interactions between HL (forms A–C) and receptors (2Q7L and 1JNX) as shown in Figures S3–S5. The two-dimensional plot curves of binding for HL (forms A–C) with the receptors (2Q7L and 1JNX) are shown in Figures S6–S8, showing bending interaction sites of HL (forms A–C) with protein active sites of receptors. Figures S6–S8 reveal that 2Q7L and 1JNX receptors cannot form hydrogen bonds with hetero atoms of HL (form B), while 2Q7L and 1JNX receptors can form bonds depending on active site of protein receptors and HL (forms A and C) as shown in Table 3.

The XRD patterns of HL and its polymer complexes (**1**–**8**) are presented in Figure 5. The XRD patterns of HL and polymer complexes **1**, **3**–**6** show many diffraction peaks which indicate polycrystalline phases. XRD patterns of polymer complexes **2**, **7** and **8** show in the range $2\theta = 20–30°$ a broad peak indicating completely amorphous structures for these polymer complexes.[20] The average crystallite size (ξ) was calculated according to the Debye–Scherrer equation:[3,28]

$$\xi = \frac{0.95\lambda}{\beta_{1/2}\cos\theta} \quad (1)$$

where $\beta_{1/2}$ is the width at half maximum of the reference diffraction peak measured in radians and λ is the wavelength of X-ray radiation (1.540598 Å). The equation uses the reference peak width at angle θ. The dislocation density (δ) is the number of dislocation lines per unit

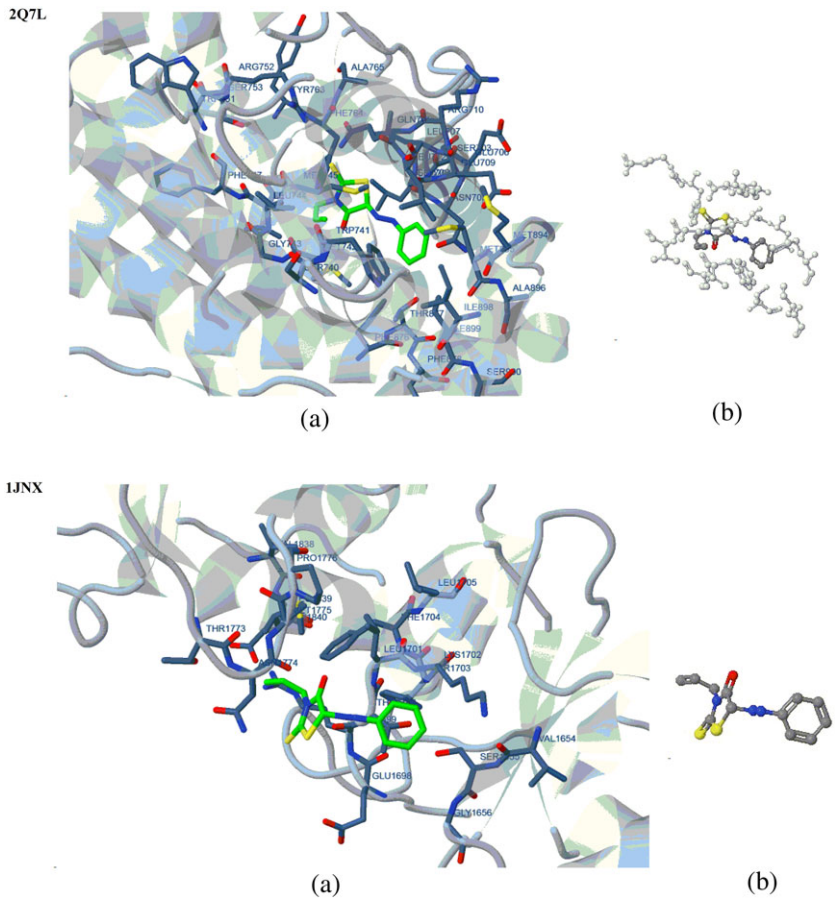

FIGURE 2 Monomer (form A) (green in (a) and grey in (b)) in interaction with receptors of 2Q7L and 1JNX

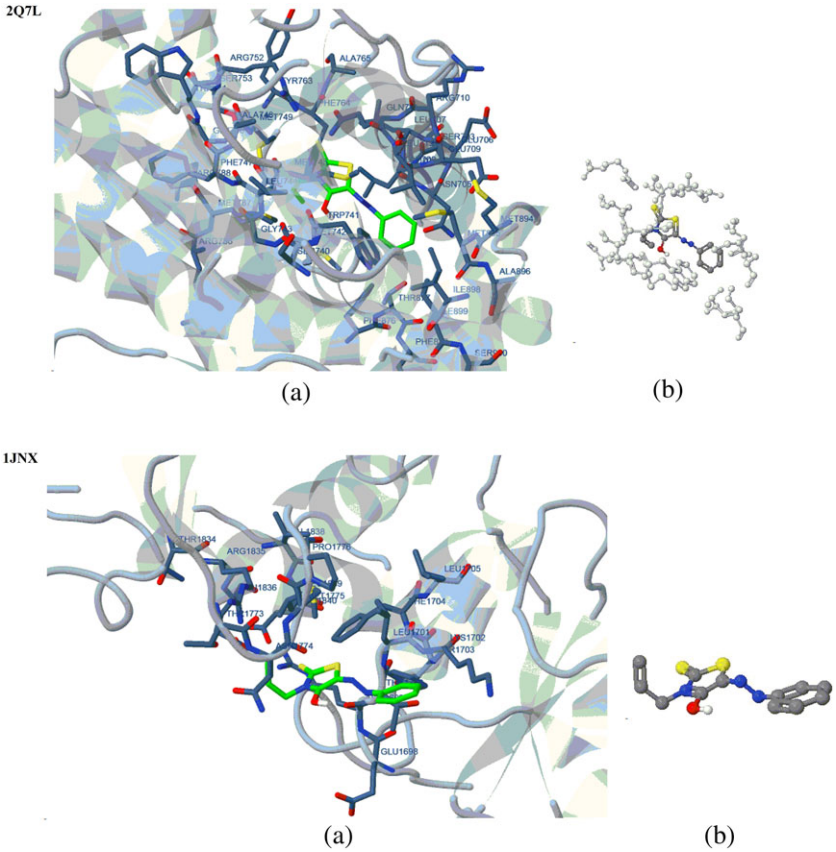

FIGURE 3 Monomer (form B) (green in (a) and grey in (b)) in interaction with receptors of 2Q7L and 1JNX

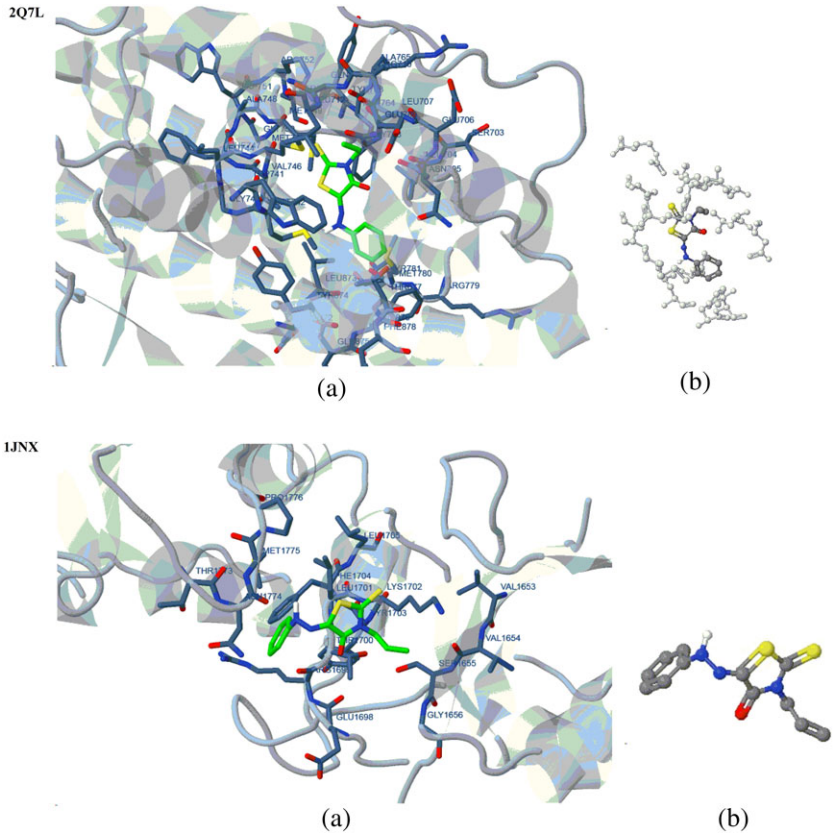

FIGURE 4 Monomer (form C) (green in (a) and grey in (b)) in interaction with receptors of 2Q7L and 1JNX

TABLE 2 Energy values obtained in docking calculations of HL (forms A–C) with receptors of prostate cancer (PDB code: 2Q7L Hormone) and breast cancer (PDB code: 1JNX Gene regulation)

Compound[a]	Receptor	Estimated free energy of binding (kcal mol^{-1})	Total intercooled energy (kcal mol^{-1})	Interaction surface
HL (form A)	2Q7L	−7.20	−8.30	517.65
	1JNX	−3.48	−6.26	550.325
HL (form B)	2Q7L	−7.22	−8.85	508.452
	1JNX	−4.45	−5.94	518.626
HL (form C)	2Q7L	−7.25	−8.73	495.055
	1JNX	−4.54	−5.82	556.472

[a]Structures are shown in Figure 1.

TABLE 3 HL (forms A and C) binding to protein with hydrogen bond interactions with receptors (2Q7L and 1JNX)

Compound[a]	Receptor	Chemical structure	Hydrogen bond[b]
HL (form A)	2Q7L	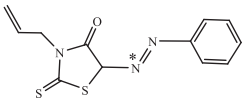	N* (3.43 Å)–LEU704 (*O*)
	1JNX	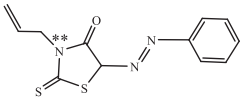	N** (2.97 Å)–ARG1699 (*O*)
HL (form C)	2Q7L	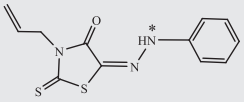	N* (3.29 Å)–MET742 (*SD*)
	1JNX	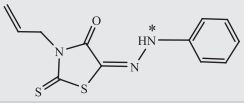	N* (2.62 Å)–ASN1774 (*O*)

[a]Structures are shown in Figure 1.

[b]Bonds as given in Figures S3–S8.

area of the crystal and calculated by the following equation:[3]

$$\delta = \frac{1}{\xi^2} \tag{2}$$

Values of ξ are 33, 31, 47, 65, 37 and 32 nm and values of δ are 9.18×10^{-4}, 1.04×10^{-3}, 4.53×10^{-4}, 2.37×10^{-4}, 7.30×10^{-4} and 9.77×10^{-4} nm^{-2} for HL and polymer complexes **1**, **3**–**6**, respectively.

The estimated lattice parameters (a, b, c, α, β and γ), Miller indices (hkl) and interplanar spacing (d) for HL and polymer complexes **1**, **3**–**6** were determined using the CHEKCELL program[31] and the data are summarized in Tables S1–S6.

The IR spectrum of the prepared HL shows a strong carbonyl absorption band appearing at *ca* 1722 cm^{-1} (Figure S9) consistent with keto hydrazone form with extensive six-membered intramolecular hydrogen bonding, since the peak appearing at *ca* 1640 cm^{-1} is attributed to ν(C=N) structure through resonance phenomena and this has been confirmed by a number of previous published data of analogous keto hydrazone. It seems that HL has different types of hydrogen bonding:[2] (i) intramolecular hydrogen bonding (Figure 1, forms B and C) and (ii) intermolecular hydrogen bonding. Case (i) is more favoured than case (ii). Also, a broad band for enolic (OH) group does not appear in the IR spectrum of monomer and the broad band located at 3114–3430 cm^{-1} leads one to characterize νNH rather than hydrogen bonded —OH with N=N, 3067 cm^{-1} (=C—H str.), 2958–3028 cm^{-1} (C—H str. —CH_2) and 2916 cm^{-1} (C—H str. sym.). This is confirmed from the observation of Karabatsos *et al.*[35] where the hydrazone form is more favoured than the azo structure for similar compounds. The low frequency and the broadness of this band suggest that the monomer has strong hydrogen bonding (N—H···O) in the solid state.[36,37] The other characteristic peaks at *ca* 1383 and 1074 cm^{-1} are due to ν(C—N) and ν(N—N) modes, respectively. Therefore, on the basis of IR data, we concluded that there is a shift of equilibrium to azo allyl rhodanine configuration and

the monomer exists in keto hydrazone form (Figure 1, form C) in the solid state.

The mode of bonding of HL to the metal ions was elucidated by comparing the IR spectra of the polymer complexes with literature data for related systems.

1. In all complexes the IR bands at *ca* 3114–3490 cm^{-1} are attributed to different probabilities: (a) due to either free NH; (b) due to bonded —NH group; or (c) due to the presence of coordinated water molecules.
2. The strong band in the IR spectrum of HL is safely assigned to ν(N—NH) vibration mode.[2] Upon complex formation with metal ions, this band is shifted to longer wavenumber as a weak band. This shows that the hydrazone group is involved in coordination in polymer complexes **1**–**4**.[10]
3. The observed new IR band assigned to ν(NH) (hydrazone) for the free HL is absent for the polymer complexes, suggesting the cleavage of intramolecular hydrogen bonded ν(NH)[38] with subsequent deprotonation of NH group and coordination of nitrogen to the metal ions as shown in polymer complexes **5**–**8**.
4. Coordination of the carbonyl oxygen and hydrazone nitrogen (NH/N) in the chelate ring is supported by the appearance of new IR bands at 550–576 and 430–446 cm^{-1} which are assigned to M—O and M—N, respectively. The phenyl ring vibration appears at 1428–1550 cm^{-1}.
5. The bands characteristic of coordinated water molecules are observed at *ca* 897 cm^{-1}, including rocking, wagging and the metal–oxygen stretching vibrations at 958, 747 and 692 cm^{-1}, respectively. The other bending vibration of the water molecules $\delta(OH_2)$, usually

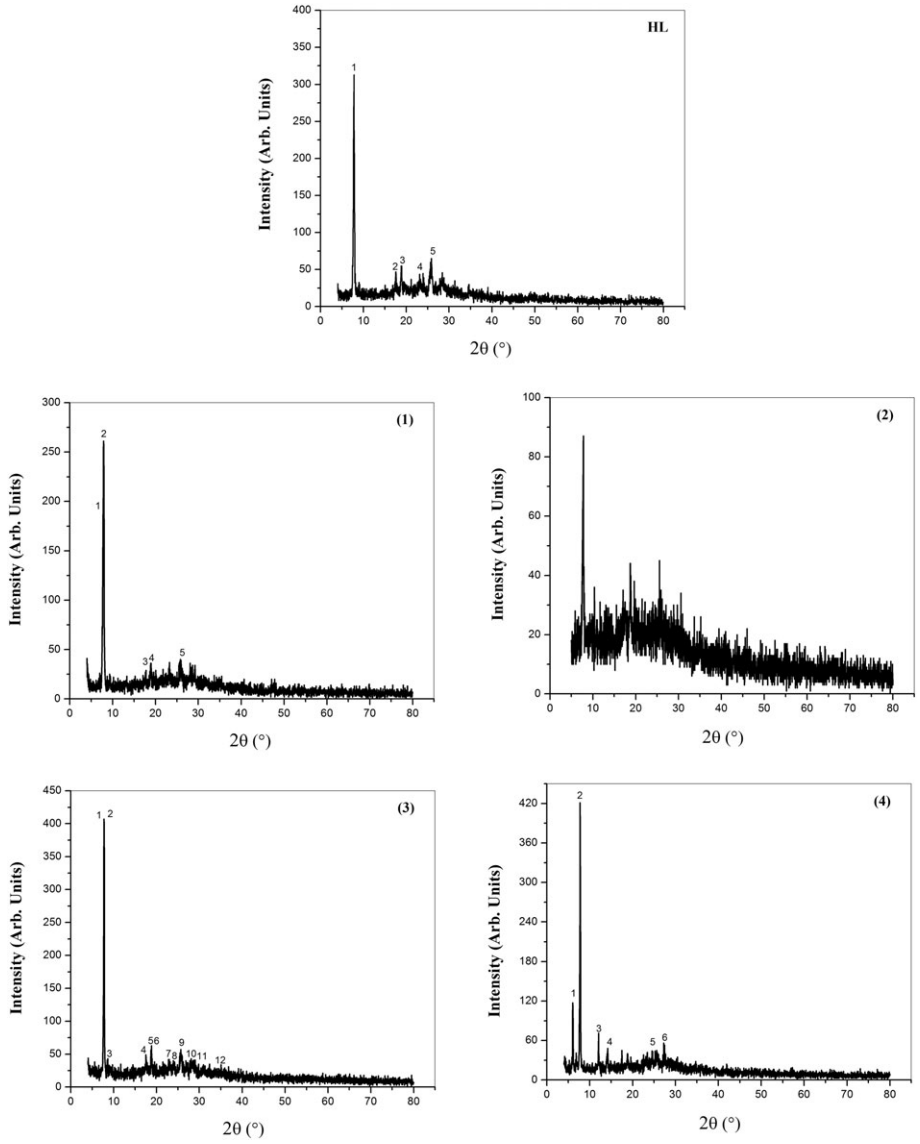

FIGURE 5 X-ray diffraction patterns of HL and polymer complexes

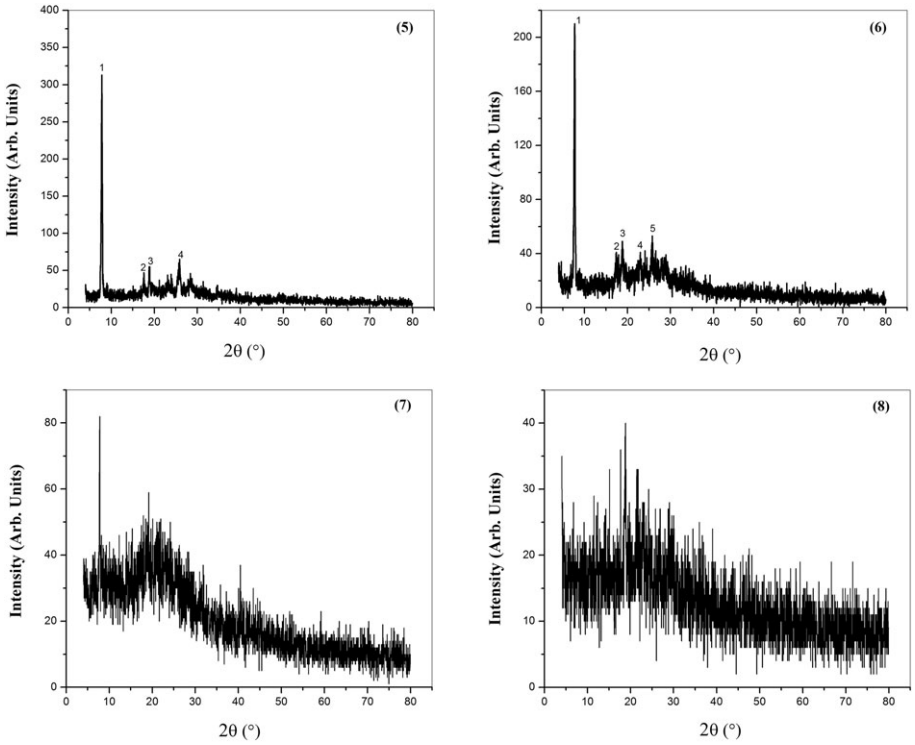

FIGURE 5 Continued.

present at *ca* 1600 cm^{-1}, is overlapped with the skeleton vibration of the benzene ring (C═C vibration).

6. The chloride test confirmed coordination for both chloride counter ions. Polymer complexes **1** and **2** react with $AgNO_3$ in HNO_3 solution. This fact is taken as evidence that chloride ions are bonded to the metal in the complex. Absorption bands at *ca* 1155–1120 cm^{-1} (ν_3), 925 cm^{-1} (ν_1), 660 cm^{-1} (ν_4) and 550 cm^{-1} (ν_2) for the sulfato polymer complexes **3** and **4** are consistent with those normally associated with bidentate chelating sulfato group.[39] In the IR spectra of the nitrato polymer complexes **5** and **6**, a value of *ca* 18 cm^{-1} for the difference between ν_5 and ν_1 indicates a bidentate mode of coordination.[40] The IR spectra of polymer complexes **7** and **8** derived from Ni(II) and Co(II) acetate show absorption bands at *ca* 1439 and 1445 cm^{-1} which are assigned to ν(C—O) antisymmetric stretching of acetate group and others at *ca* 1486 and 1493 cm^{-1} which can be assigned to ν(C—O) symmetric stretching vibration of acetate. A difference $\Delta\nu$ = 48–50 cm^{-1} indicates the mononegative bidentate coordination of the acetate group.[20,41]

3.2 | Magnetic Moments and Electronic Spectra

The results of magnetic moment measurements of all the polymer complexes are presented in Table 1. Examination of the results for these polychelates reveals that they fall in the expected range in agreement with spectral findings.

The Ni(II) polymer complexes reported herein were of high spin with room temperature magnetic moment values of μ_{eff} = 3.22–3.46 B.M. which are in the normal range observed for octahedral Ni(II) polymer complexes. This indicates that the polymer complexes of Ni(II) are six-coordinate and probably octahedral.[20,42] The electronic spectra of Ni(II) polymer complexes exhibit three d–d bands at *ca* 8400–9525 cm^{-1} (ν_1) ($^3A_{2g}(F) \rightarrow {}^2T_{2g}(F)$), 13 420–15 870 cm^{-1} (ν_2) ($^3A_{2g}(F) \rightarrow {}^3T_{1g}(F)$) and 23 800–24 400 cm^{-1} (ν_3) ($^3A_{2g}(F) \rightarrow {}^3T_{1g}(P)$), which are in the normal ranges observed for octahedral Ni(II) polymer complexes.[42] Transition energy ratio (ν_2/ν_1) obtained for all Ni(II) polymer complexes is in the range 1.64–1.70. This is indicative of octahedral geometry. The *Dq* values again confirm the octahedral configuration of the chelates.[20] The percent covalency was found to be greater for sulfato and less for acetato polymer complexes. The order of the *Dq* values among these Ni(II) polymer complexes was found to be $Cl^- < CH_3COO^- < NO_3^- < SO_4^{2-}$. Ligand field stabilization energies for the octahedral Ni(II) polymer complexes were found to have the following order: **3** > **5** > **7** > **1**.

The values of magnetic moments at room temperature for Co(II) polymer complexes lie in the range 4.40–4.92 B.M., which correspond to three unpaired electrons. The reflectance spectra of polymer complexes exhibit three absorption bands assigned to the $^4T_{1g} \rightarrow {}^4T_{2g}(F)$

(ν_1) (8300–11 904 cm^{-1}), $^4T_{1g} \rightarrow {}^4A_{2g}$ (ν_2) (15 479–18 180 cm^{-1}) and $^4T_{1g} \rightarrow {}^4T_{1g}(P)$ (ν_3) (17 543–26 660 cm^{-1}) transitions, which are in accord with octahedral geometry.[22]

The calculated values of ligand field splitting energy (10*Dq*), the Racah interelectronic repulsion parameter (*B*) and the nephelauxetic ratio (β) support the proposed geometry for all the Ni(II) and Co(II) octahedral polymer complexes. Ligand field parameter *Dq*, *B* and β were calculated for the polymer complexes and are listed in Table 4. Parameter β was calculated for the polymer complexes and the values lie in the range 0.71–0.93 cm^{-1}. These values indicate the presence of covalent character of the metal–ligand 'σ' bond. The values of the ν_2/ν_1 ratio suggest an octahedral structure for the polymer complexes.[43] The intense bands are characteristic of octahedral field around Co(II).

The nephelauxetic ratio (β) for the Ni(II) and Co(II) polymer complexes is less than one suggesting partial covalency in the metal–ligand bond. The octahedral geometry of these polymer complexes is further supported by the value of ν_2/ν_1. In general, sterically bulky ligands give rise to relatively low *Dq* values.[44] Here, the values of *Dq* obtained for our polymer complexes are relatively low which clearly show the considerable amount of bulkiness in the polymer complexes.

3.3 | Thermal Analysis

The TGA curves are shown in Figure 6 and loss of mass recorded in Table 5. The TGA curve of the monomer shows three degradation stages. The first step in the temperature range 160–281 °C is attributed to loss of $C_9H_6N_3O$ (found 61.47%; calcd 62.09%) and the second step in temperature range 281–754 °C is attributed to loss of $C_2H_5S_2$ (found 33.12%; calcd 33.58%). The third step represented the loss of one carbon atom at >754°C (mass loss: found 5.51%; calcd 4.33%).

The thermal decomposition of polymer complex **1** proceeded with two degradation stages. The first stage in the temperature range 107–252 °C is attributed to loss of two coordinated H_2O molecules and $C_8H_7NSCl_2$ (found 57.12%; calcd 57.83%).[20] The second stage at 252–800 °C is related to loss of $C_4H_4N_2S$ (found 25.36%; calcd 25.30%) and nickel oxide remained as a residue with mass percent of 17.52% (calcd 16.87%).

Polymer complex **2** decomposed in two steps. The first starts at 117–340 °C and corresponded to the loss of two coordinated H_2O molecules and $C_7H_7NSCl_2$ (found

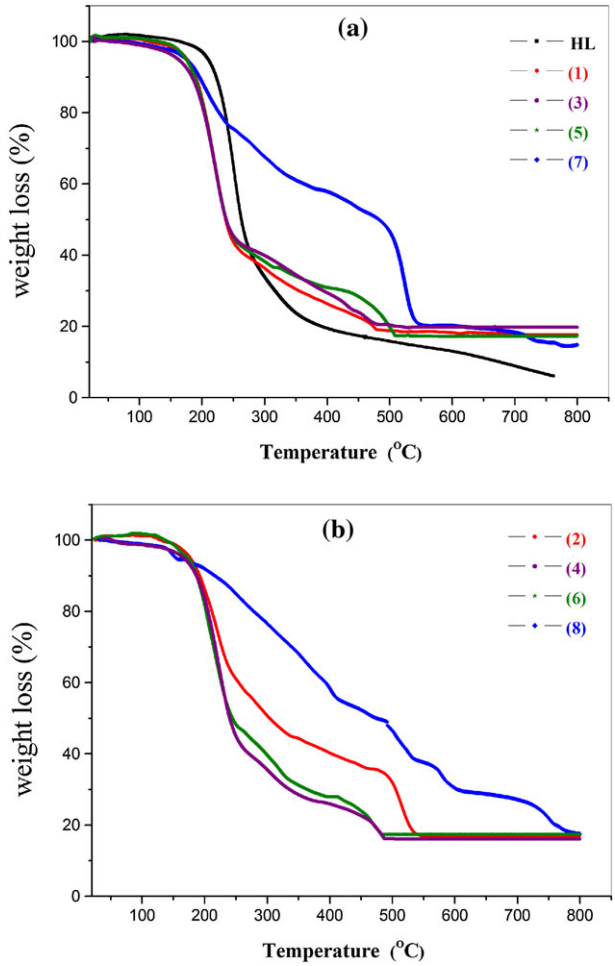

FIGURE 6 TGA curves of (a) monomer and Ni(II) polymer complexes and (b) Co(II) polymer complexes

TABLE 4 Electronic parameters of metal(II) polymer complexes

Complex	*B* (cm^{-1})	*Dq* (cm^{-1})	β	LFSE (kcal mol^{-1})	Environment
1	856	813	0.83	27.94	N, 3O, 2Cl
2	798	884	0.71	25.32	N, 3O, 2Cl
3	779	952	0.75	32.72	N, 5O
4	845	1150	0.75	32.94	N, 5O
5	799	870	0.77	29.90	N, 5O
6	1037	996	0.93	34.23	N, 5O
7	878	840	0.85	28.87	N, 5O
8	1018	1052	0.91	30.13	N, 5O

TABLE 5 TGA data for HL and polymer complexes

Compound	Temperature range (°C)	Weight loss (%) Found	Weight loss (%) Calc.	Assignment
HL	160–281	61.47	62.09	$C_9H_6N_3O$
	281–754	33.12	33.58	$C_2H_5S_2$
	>754	5.51	4.33	C
1	107–252	57.12	57.83	Coordinated $2H_2O$ molecules + $C_8H_7NSCl_2$
	252–800	25.36	25.30	$C_4H_4N_2S$
	>800	17.52	16.87	NiO
2	117–340	55.23	55.09	Coordinated $2H_2O$ molecules + $C_7H_7NSCl_2$
	340–542	27.96	27.99	$C_5H_4N_2S$
	>542	16.81	16.92	CoO
3	70–262	56.66	56.02	Coordinated $2H_2O$ molecules + $C_8H_6N_2SO_4$
	262–560	24.57	25.44	$C_3H_5NS_2$
	>560	18.77	18.54	NiO + 1C
4	40–269	59.65	60.27	Coordinated $2H_2O$ molecules + $C_7H_6N_2S_2O_4$
	269–372	13.53	14.96	C_2NS
	372–487	10.75	8.76	C_3H_5
	>487	16.07	16.01	CoO
5	125–248	54.94	54.08	Coordinated $2H_2O$ molecules + $C_7H_6N_2O_3S$
	248–507	27.54	28.66	$C_5H_4N_2S$
	>507	17.52	17.26	NiO
6	137–251	51.93	51.05	Coordinated $2H_2O$ molecules + $C_6H_5N_2O_3S$
	251–395	20.23	22.17	C_3N_2S
	395–480	10.33	9.47	C_3H_5
	>480	17.51	17.31	CoO
7	90–235	22.21	22.11	Coordinated $2H_2O$ molecules + $C_2H_3O_2$
	235–367	17.94	17.92	C_6H_5
	367–700	41.86	42.59	$C_6H_5N_3S_2$
	>700	17.99	17.38	NiO
8	60–412	44.61	42.80	Coordinated $2H_2O$ molecules + $C_9H_8O_2$
	412–610	25.90	26.98	$C_2N_2S_2$
	610–800	11.91	12.79	C_3H_5N
	>800	17.58	17.43	CoO

55.23%; calcd 55.09%). The second step represented the loss of $C_5H_4N_2S$ at 340–542 °C (found 27.96%; calcd 27.99%) and leaving CoO as a residue with mass percent of 16.81% (calcd 16.92%).

The TGA curve of polymer complex **3** showed two steps. The first stage at 70–262 °C with weight loss of 56.66% (calcd 56.02%) was consistent with the loss of two coordinated H_2O molecules and $C_8H_6N_2SO_4$. The second stage at 262–560 °C was related to loss of $C_3H_5NS_2$ (found 25.36%; calcd 25.30%) and NiO remained as a residue contaminated with one carbon atom with mass percent of 18.77% (calcd 18.54%).

The thermal decomposition of polymer complex **4** proceeded with three degradation steps within the range 40 to 487 °C. The first started at 40–269 °C and corresponded to the loss of two coordinated H_2O molecules and $C_7H_6N_2S_2O_4$ (found 59.65%; calcd 60.27%). The second and third steps represented the loss of remaining monomer molecules (C_2NS and C_3H_5) at 269–487 °C (found 24.28%; calcd 23.72%), with CoO as a residue with mass percent of 16.07% (calcd 16.01%).

The TGA curve of polymer complex **5** showed two stages of decomposition. The first stage at 125–248 °C corresponded to the loss of two coordinated H_2O molecules and $C_7H_6N_2O_3S$ with a weight loss of 54.94% (calcd 54.08%) and the second stage at 248–507 °C was related to loss of $C_5H_4N_2S$ (found 27.54%; calcd 28.66%). Nickel oxide remained as a residue with mass percent of 17.52% (calcd 17.26%).

The thermal decomposition of polymer complex **6** proceeded with three degradation stages. The first stage in the range 137–251 °C was attributed to loss of two coordinated H_2O molecules and $C_6H_5N_2O_3S$ (found 51.93%; calcd 51.05%),[20] the second stage at 251–395 °C was related to loss of C_3N_2S (found 20.23%; calcd 22.17%) and the third stage at 395–480 °C correlated with elimination of C_3H_5

(found 10.33%; calcd 9.47%), with cobalt oxide as a residue with mass percent of 17.51% (calcd 17.31%).

Polymer complex **7** showed three decomposition steps within the range 90–800 °C. The first decomposition step within the temperature range 90–235 °C corresponded to the loss of two coordinated H_2O molecules and $C_2H_3O_2$ (found 22.21%; calcd 22.11%)[20] and the second decomposition step at 235–367 °C was related to loss C_6H_5 (found 17.94%; calcd 17.92%). The third step (367–700 °C) corresponded to $C_6H_5N_3S_2$ with a mass loss of 41.86% (calcd 42.59%), and leaving NiO as a residue with mass percent of 17.99% (calcd 17.38%).

The thermogram of polymer complex **8** showed three decomposition steps within the range 60–800 °C. The first decomposition step within the range 60–412 °C corresponded to the loss of two coordinated H_2O molecules and $C_9H_8O_2$ with a mass loss of 44.61% (calcd 42.80%) and the second decomposition step at 412–610 °C was related to loss of $C_2N_2S_2$ (found 25.90%; calcd 26.98%). The third step (610–800 °C) corresponded to the removal of remaining part of the monomer (C_3H_5N) with a mass loss of 11.91% (calcd 12.79%), and leaving CoO as a residue with mass percent of 17.58% (calcd 17.43%).

TABLE 6 Thermodynamic data for thermal decomposition of HL and polymer complexes

Compound	Decomposition temperature (°C)	Method[a]	Thermodynamic parameters				Correlation coefficient
			E_a (kJ mol^{-1})	ΔS^* (J mol^{-1} K^{-1})	ΔH^* (kJ mol^{-1})	ΔG^* (kJ mol^{-1})	
HL	160–281	CR	107	−86.9	103	146	0.99484
		HM	116	−52.5	112	138	0.99916
	281–450	CR	41.9	−233	36.6	186	0.98993
		HM	52.8	−218	47.5	187	0.99613
1	147–252	CR	37.8	−191	33.9	124	0.99433
		HM	39.9	−211	35.9	136	0.98758
	252–477	CR	78.6	−199	73.3	200	0.99716
		HM	85.5	−162	80.2	184	0.99402
2	117–340	CR	34.1	−200	30.0	130	0.99749
		HM	38.2	−221	34.0	145	0.99593
	464–542	CR	91.6	−201	85.1	241	0.99605
		HM	94.6	−179	88.1	227	0.99799
3	140–262	CR	86.9	−115	83.0	137	0.9995
		HM	95.4	−87.1	91.5	133	0.99545
	262–481	CR	99.8	−188	94.4	216	0.99401
		HM	102	−136	97.1	185	0.99393
4	148–269	CR	83.6	−109	79.6	132	0.99441
		HM	90.9	−100	86.9	135	0.99798
	372–525	CR	132	−118	126	211	0.99073
		HM	145	−94.9	139	207	0.99065
5	147–400	CR	39.2	−234	34.7	162	0.99501
		HM	43.6	−219	39.1	158	0.99737
	400–509	CR	131	−105	125	201	0.99679
		HM	141	−102	135	209	0.99782
6	137–251	CR	36.7	−227	32.8	139	0.99695
		HM	40.1	−209	36.3	134	0.96607
	395–517	CR	122	−142	115	219	0.99088
		HM	133	−113	127	210	0.99385
7	140–387	CR	35.7	−236	31.2	158	0.99494
		HM	44.3	−215	39.9	155	0.99199
	387–552	CR	124	−143	118	224	0.99667
		HM	134	−116	128	214	0.99593
8	100–412	CR	28.9	−255	24.5	159	0.99777
		HM	38.5	−226	34.1	154	0.99633
	665–797	CR	95.7	−206	87.3	294	0.99912
		HM	106	−200	97.9	299	0.99785

[a]CR, Coats–Redfern; HM, Horowitz–Metzger.

3.4 | Kinetic Studies

The thermodynamic parameters for HL and its polymer complexes, namely enthalpy (ΔH^*), thermal activation energy of decomposition (E_a), Gibbs free energy change of decomposition (ΔG^*) and entropy (ΔS^*), are calculated using the Coats–Redfern and Horowitz–Metzger methods.[45,46] ΔH^* and ΔG^* were calculated using $\Delta H^* = E_a - RT$ and $\Delta G^* = \Delta H^* - T\Delta S^*$, respectively. The thermodynamic data obtained with the Coats–Redfern and Horowitz–Metzger methods for HL and polymer complexes **1**–**8** are shown in Figures S10 and S11 and the thermodynamics parameters are summarized in Table 6. The data obtained from the two methods are comparable and can be considered in good agreement with each other.[28] The data obtained are summarized in the following:

1. The E_a values of the polymer complexes are less than that of HL.
2. The E_a value of polymer complex **1** is higher than those of the other complexes.
3. ΔG^* values for HL and its polymer complexes are positive and confirmed the process is non-spontaneous.
4. ΔS^* values of HL and its polymer complexes are negative indicating the reaction is slow or the activated complex is more ordered than the reactants.[3,20]
5. The effect of the different metals on E_a is shown in Figure 7. It was found that the values of E_a for Ni(II) polymer complexes are greater than those for Co(II) polymer complexes.[28]

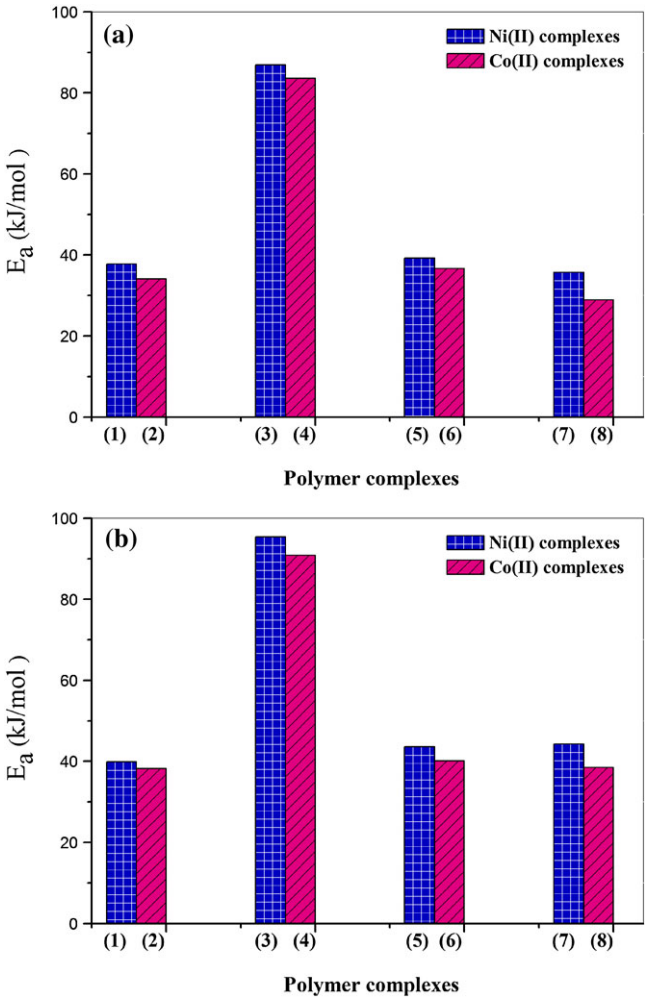

FIGURE 7 Histograms of thermal activation energy of decomposition data for Ni(II) and Co(II) polymer complexes: (a) Coats–Redfern method; (b) Horowitz–Metzger method

3.5 | DNA Binding Studies

DNA is a major target for drugs, and studies of the nature of the binding of these small molecules to DNA are important and fundamental for life sciences.[47,48] DNA is one of the most important biomacromolecules in life processes because it carries inheritance information and instructs biological synthesis.[3,49]

TABLE 7 Intrinsic binding constants (K_b) of HL and polymer complexes

Compound	K_b (M^{-1})
HL	9.96×10^4
1	2.49×10^5
2	2.31×10^5
3	3.09×10^5
4	2.89×10^5
5	2.87×10^5
6	2.56×10^5
7	1.14×10^5
8	1.01×10^5

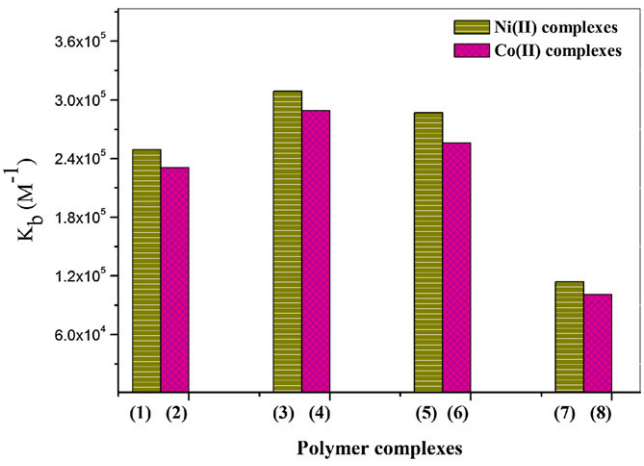

FIGURE 8 Histogram of intrinsic binding constant (K_b) values for Ni(II) and Co(II) polymer complexes

The intercalation of monomer and polymer complexes with CT-DNA was investigated using absorption spectroscopy to determine the intrinsic binding constant (K_b). In the presence of DNA, the absorption bands of HL and polymer complexes **1**–**8** at about 425, 417, 423, 396, 399, 391, 417, 422 and 421 nm, respectively, exhibited hypochromism and a red shift of about 1–3 nm (Figure S12). It was found that the absorption bands of HL and its polymer complexes decrease with increasing concentration of CT-DNA.[3,28] K_b of HL and its polymer complexes is determined using the following equation:[28]

$$\frac{[\mathrm{DNA}]}{\varepsilon_a - \varepsilon_f} = \frac{[\mathrm{DNA}]}{\varepsilon_b - \varepsilon_f} + \frac{1}{K_b(\varepsilon_a - \varepsilon_f)} \quad (3)$$

where ε_a is the molar extinction coefficient observed for A_{obs}/[monomer or polymer complex] at a specific DNA concentration, ε_f is the molar extinction coefficient of the free monomer or polymer complex in solution, [DNA] is the concentration of CT-DNA in base pairs and ε_b is the molar extinction coefficient of the monomer or polymer complex when fully bound to DNA. Plots of [DNA]/($\varepsilon_a - \varepsilon_f$) versus [DNA] (Figure S12) were used to determine K_b.

The K_b values were calculated and are recorded in Table 7. The Ni(II) polymer complexes (**1**, **3**, **5** and **7**) have the highest values of K_b (Figure 8), indicating that the Ni(II) polymer complexes more strongly bind with CT-DNA which can be due to the lower ionic radius of Ni(II) compared to Co(II).[28,50,51]

TABLE 8 Antibacterial activity of monomer and polymer complexes[a]

		Gram-positive bacteria			Gram-negative bacteria		
Compound	**Conc. (μg/ml)**	***Bacillus cereus***	***Staphylococcus aureus***	***Enterococcus faecalis***	***Escherichia coli***	***Klebsiella pneumoniae***	***Pseudomonas aeruginosa***
HL	50	−ve	−ve	−ve	−ve	−ve	−ve
	100	−ve	−ve	−ve	2.0 ± 0	−ve	−ve
	150	−ve	−ve	−ve	2.0 ± 0	−ve	−ve
1	50	−ve	−ve	−ve	−ve	−ve	−ve
	100	−ve	0.4 ± 0	−ve	−ve	−ve	−ve
	150	−ve	0.6 ± 0	−ve	−ve	−ve	−ve
2	50	−ve	−ve	−ve	−ve	0.2 ± 0[b]	−ve
	100	−ve	−ve	−ve	−ve	0.2 ± 0[b]	−ve
	150	−ve	−ve	−ve	−ve	0.2 ± 0[b]	−ve
3	50	0.4 ± 0	−ve	−ve	0.2 ± 0	−ve	−ve
	100	0.6 ± 0	0.4 ± 0	−ve	0.2 ± 0	−ve	−ve
	150	0.8 ± 0	0.35 ± 0.04	−ve	0.4 ± 0	−ve	−ve
4	50	−ve	−ve	−ve	0.3 ± 0	−ve	−ve
	100	−ve	0.2 ± 0	−ve	0.3 ± 0	−ve	−ve
	150	−ve	0.4 ± 0	−ve	0.3 ± 0	−ve	−ve
5	50	−ve	0.4 ± 0	−ve	0.4 ± 0	−ve	−ve
	100	−ve	0.77 ± 0.06	−ve	0.4 ± 0	−ve	0.33 ± 0.033
	150	0.4 ± 0	0.88 ± 0.02	−ve	0.5 ± 0	−ve	0.33 ± 0.033
6	50	−ve	−ve	−ve	−ve	−ve	0.40 ± 0
	100	−ve	0.2 ± 0	−ve	−ve	−ve	0.47 ± 0.033
	150	−ve	0.2 ± 0	−ve	−ve	−ve	0.53 ± 0.033
7	50	0.2 ± 0	−ve	−ve	0.4 ± 0	−ve	−ve
	100	0.4 ± 0	−ve	−ve	0.6 ± 0	−ve	−ve
	150	0.4 ± 0	−ve	−ve	0.6 ± 0	−ve	−ve
8	50	−ve	−ve	−ve	0.2 ± 0	−ve	−ve
	100	−ve	−ve	−ve	0.2 ± 0	−ve	−ve
	150	0.2 ± 0	−ve	−ve	0.6 ± 0	−ve	−ve
Penicillin (standard drug)	50	1 ± 0.14	2 ± 0	1.46 ± 0.03	1 ± 0	−ve	0.87 ± 0.033
	100	3 ± 0.28	2 ± 0.14	1.86 ± 0.03	3 ± 0	−ve	1.06 ± 0.033
	150	3 ± 0.14	2 ± 0	2.2 ± 0	3 ± 0	−ve	1.4 ± 0.058

[a]Data recorded as average diameter of inhibition zone (mm) ± standard deviation.

[b]Indicates significantly different value from that of penicillin.

TABLE 9 Antifungal activity of monomer and polymer complexes[a]

Compound	Conc. (μg/ml)	*Aspergillus niger*	*Fusarium oxysporum*	*Candida albicans*
HL	50	−ve	−ve	−ve
	100	−ve	−ve	−ve
	150	−ve	−ve	−ve
1	50	−ve	−ve	−ve
	100	0.9 ± 0.1	0.6 ± 0	−ve
	150	0.9 ± 0	0.6 ± 0	−ve
2	50	−ve	0.2 ± 0	−ve
	100	−ve	0.3 ± 0.1	−ve
	150	−ve	0.8 ± 0	−ve
3	50	−ve	−ve	−ve
	100	−ve	−ve	−ve
	150	0.8 ± 0	−ve	−ve
4	50	−ve	0.4 ± 0	−ve
	100	−ve	0.6 ± 0	−ve
	150	−ve	1 ± 0	−ve
5	50	−ve	−ve	−ve
	100	−ve	−ve	−ve
	150	−ve	−ve	−ve
6	50	−ve	0.4 ± 0	−ve
	100	−ve	1 ± 0	−ve
	150	−ve	1 ± 0	−ve
7	50	−ve	−ve	−ve
	100	−ve	−ve	−ve
	150	−ve	−ve	−ve
8	50	−ve	−ve	−ve
	100	−ve	−ve	−ve
	150	−ve	−ve	−ve
Miconazole (standard drug)	50	1 ± 0	2 ± 0	1.1 ± 0
	100	3 ± 0.14	3 ± 0	1.3 ± 0
	150	4 ± 0	3 ± 0	1.7 ± 0.058

[a]Data recorded as average diameter of inhibition zone (mm) ± standard deviation.

3.6 | Antimicrobial Studies

Antifungal and antibacterial activities of the monomer and polymer complexes were investigated. The data are presented in Tables 8 and 9. Polymer complexes and monomer have no antibacterial activity against *E. faecalis* and *K. pneumoniae* except Co(II) polymer complex **2** that has antibacterial activity against *K. pneumoniae*, being more active than penicillin which was used as standard antibacterial drug. The monomer was found to have antibacterial activity against *E. coli* and has no antibacterial activity against *P. aeruginosa*, *K. pneumoniae*, *S. aureus*, *B. cereus* and *E. faecalis*.

Polymer complex **1** has antibacterial activity against *S. aureus* and has no antibacterial activity against *E. coli*, *K. pneumoniae*, *B. cereus*, *E. faecalis* and *P. aeruginosa*. Polymer complex **3** has antibacterial activity against *B. cereus*, *S. aureus* and *E. coli* and has no antibacterial activity against *E. faecalis*, *K. pneumoniae* and *P. aeruginosa* (Table 8). Also, Ni(II) polymer complex **5** has antibacterial activity against *B. cereus*, *S. aureus*, *E. coli* and *P. aeruginosa* and has no antibacterial activity against *E. faecalis* and *K. pneumoniae*. Ni(II) polymer complex **7** has antibacterial activity against *B. cereus*, and *E. coli* and has no antibacterial activity against *S. aureus*, *E. faecalis*, *K. pneumoniae* and *P. aeruginosa*.

Co(II) polymer complex **2** has antibacterial activity against *K. pneumoniae* and has no antibacterial activity against *B. cereus*, *S. aureus*, *E. faecalis*, *E. coli* and *P. aeruginosa*. Co(II) polymer complex **2** is more active than penicillin against *K. pneumoniae*. The antibacterial activity of Co(II) polymer complex **2** may be because of there being two chloride ions and because of the type of metal. Polymer complex **4** has antibacterial activity against *E. coli* and *S. aureus* and has no antibacterial activity against *B. cereus*, *E. faecalis*, *K. pneumoniae* and *P. aeruginosa* (Table 8). Co(II) polymer complex **6** has antibacterial activity against *S. aureus* and *P. aeruginosa* and has no

antibacterial activity against *B. cereus*, *E. faecalis*, *E. coli* and *K. pneumoniae*. Co(II) polymer complex **8** has antibacterial activity against *B. cereus* and *E. coli* and has no antibacterial activity against *S. aureus*, *E. faecalis*, *K. pneumoniae* and *P. aeruginosa*. In addition, polymer complexes **5** and **6** have moderate antibacterial activity against *P. aeruginosa* when compared to penicillin.

The results of the antifungal activities of the monomer and its polymer complexes are recorded in Table 9. The results reveal that polymer complex **1** is moderately toxic against *A. niger* and *F. oxysporum*, whereas it has no anticandidal activity. Polymer complex **3** has a small effect against *A. niger* and has no antifungal activity against *F. oxysporum* and no anticandidal activity. Our results are similar to those of Habib *et al.*[52] who studied the antimicrobial activities of some rhodanine derivatives and they revealed that the most pronounced antifungal activity was against *A. niger* and *Penicillium* sp.

Co(II) polymer complex **2** is of low toxicity against *F. oxysporum* and Co(II) polymer complexes **4** and **6** are of high toxicity against *F. oxysporum*. Co(II) polymer complexes **2**, **4** and **6** have no antifungal activity against *A. niger* and *C. albicans*. The monomer, Ni(II) polymer complexes **5** and **7** and Co(II) polymer complex **8** have no antifungal activity against *A. niger*, *F. oxysporum* and *C. albicans*.

4 | CONCLUSIONS

A series of Ni(II) and Co(II) polymer complexes with monomer HL were prepared and characterized. The coordination behavior of the anions in the Ni(II) and Co(II) polymer complexes was also discussed on the basis of IR spectral and molar conductance measurements. It was observed that the coordination of anions with metal was effected via a number of coordination sites, which was further confirmed by molar conductance. The geometries of the polymer complexes are also affected by the number of coordination sites and monomer (HL).

1. It is also clear that the monomer has high affinity for chelation with the metal ions under study due to the increasing charge density of the metal ions and hence to the increasing of their coordination affinities.
2. The formulae $[M(HL)(Cl)_2(OH_2)_2]_n$, $[M(HL)(O_2SO_2)(OH_2)_2]_n$, $[M(L)(O_2NO)(H_2O)_2]_n$ and $[M(L)(O_2CCH_3)(H_2O)_2]_n$ (where M = Ni(II) or Co(II)) have been proposed on the basis of analytical and various physicochemical data. The hydrazone moiety is bonded to the metal ions in neutral/monobasic bidentate manner through NH/N (hydrazone) group and carbonyl oxygen as inferred from IR spectra.
3. The value of thermal activation energy of decomposition for monomer is higher compared to the polymer complexes.

ACKNOWLEDGEMENT

The authors thank Prof. Dr M.I. Abou-Dobara, Botany Department, Faculty of Science, Damietta University, Egypt for his help during investigation of antimicrobial activity.

ORCID

Sh. M. Morgan http://orcid.org/0000-0002-8921-4894
A. Z. El-Sonbati http://orcid.org/0000-0001-7059-966X

REFERENCES

[1] A. Z. El-Sonbati, A. A. M. Belal, M. A. Diab, M. Z. Balboula, *Spectrochim. Acta A* **2011**, *78*, 1119.

[2] M. A. Diab, A. Z. El-Sonbati, A. A. El-Bindary, M. Z. Balboula, *J. Mol. Struct.* **2013**, *1040*, 171.

[3] A. Z. El-Sonbati, M. A. Diab, Sh. M. Morgan, M. Z. Balboula, *Appl. Organometal. Chem.* **2017**, https://doi.org/10.1002/aoc.4059.

[4] N. A. El-Ghamaz, M. A. Diab, A. Z. El-Sonbati, Sh. M. Morgan, O. L. Salem, *Chem. Pap.* **2017**, *71*, 2417.

[5] M. A. Diab, A. Z. El-Sonbati, R. H. Mohamed, *Spectrochim. Acta A* **2010**, *77*, 795.

[6] P. Tang, W. W. Dong, W. Xia, J. Zhao, *J. Inorg. Organometal. Polym.* **2015**, *25*, 569.

[7] A. Z. El-Sonbati, A. A. M. Belal, M. S. El-Gharib, Sh. M. Morgan, *Spectrochim. Acta A* **2012**, *95*, 627.

[8] A. Z. El-Sonbati, M. A. Diab, A. A. M. Belal, Sh. M. Morgan, *Spectrochim. Acta A* **2012**, *99*, 353.

[9] A. Z. El-Sonbati, M. A. Diab, A. A. M. Belal, M. E. Attallah, *Spectrochim. Acta A* **2012**, *86*, 547.

[10] A. Z. El-Sonbati, M. A. Diab, M. S. El-Shehawy, M. Moqbal, *Spectrochim. Acta A* **2010**, *75*, 394.

[11] A. Z. El-Sonbati, M. A. Diab, M. M. El-Halawany, N. E. Salam, *Spectrochim. Acta A* **2010**, *77*, 755.

[12] M. I. Abou-Dobara, A. Z. El-Sonbati, Sh. M. Morgan, *World J. Microbiol. Biotechnol.* **2013**, *29*, 119.

[13] W. I. Stephen, A. Townshend, *Anal. Chim. Acta* **1965**, *33*, 257.

[14] G. G. Alfonso, J. L. Gomez Ariza, *Microchem. J.* **1981**, *26*, 574.

[15] W. T. Sing, C. L. Lee, S. L. Yeo, S. P. Lim, M. M. Sim, *Bioorg. Med. Chem. Lett.* **2001**, *11*, 91.

[16] Q.-P. Wu, L. Zhang, M. Liang, Z. Sun, S. Xue, *Solar Energy* **2011**, *85*, 1.

[17] J. Yu, L. Ge, P. Dai, S. Ge, S. Liu, *Biosens. Bioelectron.* **2010**, *25*, 2065.

[18] J.-h. Yu, P. Dai, S.-g. Ge, Y.-n. Zhu, L.-n. Zhang, X.-l. Cheng, *Spectrochim. Acta A* **2009**, *72*, 17.

[19] J.-h. Yu, F.w. Wan, P. Dai, S.-g. Ge, B. Li, J.-d. Huang, *Anal. Lett.* **2009**, *42*, 746.

[20] A. Z. El-Sonbati, M. A. Diab, Sh. M. Morgan, *J. Mol. Liq.* **2017**, *225*, 195.

[21] F. Meyer, H. Kozlowski, in *Comprehensive Coordination Chemistry II*, (Eds: J. A. McCleverty, T. J. Meyer) Vol. 6, Elsevier, Amsterdam **2003** 247.

[22] R. L. Kurtaran, L. T. Yildirim, A. D. Azaz, H. Namli, O. Atakol, *J. Inorg. Biochem.* **2005**, *99*, 1937.

[23] W. Luo, X. Meng, X. Sun, F. Xiao, J. Shen, Y. Zhou, G. Cheng, Z. Ji, *Inorg. Chem. Commun.* **2007**, *10*, 1351.

[24] Z. Afrasiabi, E. Sinn, W. Lin, Y. Ma, C. Campana, S. Padhye, *J. Inorg. Biochem.* **2005**, *99*, 1526.

[25] M. Maghami, F. Farzaneh, J. Simpson, M. Ghiasi, M. Azarkish, *J. Mol. Struct.* **2015**, *1093*, 24.

[26] A. Z. El-Sonbati, M. A. Diab, A. A. El-Bindary, A. M. Eldesoky, S. M. Morgan, *Spectrochim. Acta A* **2015**, *135*, 774.

[27] R. C. Maurya, B. A. Malik, J. M. Mir, P. K. Vishwakarma, D. K. Rajak, N. Jain, *J. Mol. Struct.* **2015**, *5*, 266.

[28] Sh. M. Morgan, A. Z. El-Sonbati, H. R. Eissa, *J. Mol. Liq.* **2017**, *240*, 752.

[29] N. A. El-Ghamaz, A. Z. El-Sonbati, Sh. M. Morgan, *J. Mol. Struct.* **2012**, *1027*, 92.

[30] Sh. M. Morgan, M. A. Diab, A. Z. El-Sonbati, *Appl. Organometal. Chem.* **2018**, https://doi.org/10.1002/aoc.4281

[31] R. Shirley, *The CRYSFIRE System for Automatic Powder Indexing: User's Manual*, Lattice Press, Guildford **2000**.

[32] J. Laugier, B. Bochu, LMGP suite of programs for the interpretation of X-ray experiments, ENSP/Laboratoire des Materiaux et du Genie Physique, Saint Martin d'Heres, **2000**.

[33] G. G. Mohamed, A. A. El-Sherif, M. A. Saad, S. E. A. El-Sawy, Sh. M. Morgan, *J. Mol. Liq.* **2016**, *223*, 1311.

[34] H. M. Refaat, H. A. El-Badway, Sh. M. Morgan, *J. Mol. Liq.* **2016**, *220*, 802.

[35] G. J. Karabatsos, B. L. Shapiro, F. M. Vane, J. S. Fleming, J. S. Ratka, *J. Am. Chem. Soc.* **1963**, *85*, 2784.

[36] S. Wang, S. Shen, H. Xu, *Dyes Pigm.* **2000**, *44*, 195.

[37] D. Maiti, H. Paul, N. Chanda, S. Chakraborty, B. Mondal, V. G. Puranik, G. K. Lahiri, *Polyhedron* **2004**, *23*, 831.

[38] A. Z. El-Sonbati, A. A. Al-Sarawy, M. Moqbel, *Spectrochim. Acta A* **2009**, *74*, 463.

[39] K. Nakamoto, *Infrared and Raman Spectra of Inorganic and Coordination Compounds*, 3rd ed., Wiley-Interscience, New York **1978**.

[40] E. Abdel-Latif, *Phosphorus Sulfur Silicon* **2006**, *181*, 125.

[41] K. Nakamoto, *Infrared and Raman Spectra of Inorganic and Coordination Compounds*, Wiley Interscience, New York **1986**.

[42] F. A. Cotton, G. Wilkinson, C. A. Murillo, M. Bpchimann, *Advanced Inorganic Chemistry*, 6th ed., Wiley, New York **1999**.

[43] A. B. P. Lever, E. Mantovani, *Inorg. Chem.* **1971**, *10*, 817.

[44] A. P. B. Lever, *Inorganic Electronic Spectroscopy*, 2nd ed., Elsevier, New York **1985**.

[45] A. W. Coats, J. P. Redfern, *Nature* **1964**, *201*, 68.

[46] H. H. Horowitz, G. Metzger, *Anal. Chem.* **1963**, *35*, 1464.

[47] X. H. Zhang, L. Y. Wang, Z. X. Nan, S. H. Tan, Z. X. Zhang, *Dyes Pigm.* **2008**, *79*, 205.

[48] K. L. Reddy, K. R. Y. Harish, K. K. Ashwini, S. S. S. Vidhisha, *Nucleos. Nucleot. Nucl.* **2009**, *28*, 204.

[49] A. Z. El-Sonbati, M. A. Diab, Sh. M. Morgan, A. M. Eldesoky, M. Z. Balboula, *Appl. Organometal. Chem.* **2018**, https://doi.org/10.1002/aoc.4207.

[50] S. Mondal, B. Pakhira, A. J. Blake, M. G. B. Drew, S. K. Chattopadhyay, *Polyhedron* **2016**, *117*, 327.

[51] A. Z. El-Sonbati, M. A. Diab, Sh. M. Morgan, H. A. Seyam, *J. Mol. Struct.* **2018**, *1154*, 354.

[52] N. S. Habib, S. M. Rida, E. A. M. Badawey, H. T. Y. Fahmy, H. A. Ghozlan, *Eur. J. Med. Chem.* **1997**, *32*, 759.

SUPPORTING INFORMATION

Additional Supporting Information may be found online in the supporting information tab for this article.

How to cite this article: Morgan ShM, El-Sonbati AZ, El-Mogazy MA. Polymer complexes. LXX. Synthesis, spectroscopic studies, thermal properties and antimicrobial activity of metal(II) polymer complexes. *Appl Organometal Chem*. 2018;e4264. https://doi.org/10.1002/aoc.4264